Sheffield Hallam University

Competition of lattice and spin excitations in the temperature dependence of spin-wave properties

DI GENNARO, Marco, MIRANDA, Alonso L, OSTLER, Thomas <http://orcid.org/0000-0002-1328-1839>, ROMERO, Aldo H and VERSTRAETE, Matthieu J

Citation:

Copyright and re-use policy

Competition of lattice and spin excitations in the temperature dependence of spin-wave properties

Marco Di Gennaro,[1,*] Alonso L. Miranda,[2] Thomas A. Ostler,[1,3] Aldo H. Romero,[4,5] and Matthieu J. Verstraete[1]

[1]*nanomat/Q-MAT/CESAM and European Theoretical Spectroscopy Facility, Université de Liège, B-4000 Liège, Belgium*
[2]*CINVESTAV, Departamento de Materiales, Unidad Querétaro, Querétaro 76230, México*
[3]*Faculty of Arts, Computing, Engineering and Sciences, Sheffield Hallam University, Howard Street, Sheffield S1 1WB, United Kingdom*
[4]*Physics and Astronomy Department, West Virginia University, Morgantown, West Virginia 26506, USA*
[5]*Facultad de Ingeniería, Benemérita Universidad Autnoma de Puebla, 72570 Puebla, Pue., México*

The interplay of magnons and phonons can induce strong temperature variations in the magnetic exchange interactions, leading to changes in the magnetothermal response. This is a central mechanism in many magnetic phenomena, and in the new field of Spin Caloritronics, which focuses on the combination of heat and spin currents. Boson model systems have previously been developed to describe the magnon-phonon coupling but, until recently, studies rely on empirical parameters. In this paper, we propose a first-principles approach to describe the dependence of the magnetic exchange integrals on phonon renormalization, leading to changes in the magnon dispersion as a function of temperature. The temperature enters into the spin dynamics (by introducing fluctuations) as well as in the magnetic exchange itself. Depending on the strength of the coupling, these two temperatures may or may not be equilibrated, yielding different regimes. We test our approach in typical and well-known ferromagnetic materials: Ni, Fe, and Permalloy. We compare our results to recent experiments on the spin-wave stiffness, and discuss departures from Bloch's law and parabolic dispersion.

I. INTRODUCTION

The interaction of ionic vibrational and magnetic degrees of freedom (magnon-phonon coupling or MPC) influences many physical properties in magnetic and strongly correlated materials. Beyond providing a playground to fundamental science, MPC holds promise in many applied fields such as nanoelectronics (to boost efficiency and reduce power consumption), sensors and actuators (magnetothermal response can be combined with multiple external inputs: B field, T, strain, current...), or to reduce magnetotransport response: spin currents can experience reduced resistance due to coupling with coherent acoustic vibrations, giving resonant magnetoelastic deformations. The explicit calculation, and then engineering, of MPC will be central to the development of devices operating at room temperature and above.

Since the 1950s, MPC has been studied using model Hamiltonians [1–4]. Only very recently, Fransson *et al.* [5] have published a more complete theory of MPC interaction terms and their possible symmetries. The interaction governs changes in the frequency and relaxation time of magnons as a function of temperature, and conversely the change in phonon frequencies and lifetimes with the magnetic state. Over the past decade, the physics of electrical to spin transport conversion has expanded dramatically [6–10]. The new field of Spin Caloritronics characterizes different transport phenomena, which depend on the coupling between thermal vibrations, charge, and spin [11,12]. Creative experiments have led to the discovery of new physical effects (Spin Peltier, Spin Seebeck, Spin-dependent Seebeck, etc.), which combine temperature gradients, internal and external magnetic fields, heat currents, charge, and spin, and in which energy conversion depends (at least in part) on intrinsic magnetic excitations, along with their coupling to phonons and electrons. Conversely, temperature can also have a strong *direct* effect on the magnetic excitations themselves, as demonstrated, e.g., in Ni deposited on VO_2, where heat drives a softening of a VO_2 phonon mode, which couples to the magnetic response in Ni [13].

MPC is much more delicate than electron-phonon coupling, as the quasiparticles can have similar energies and momenta—neither is a universally small perturbation of the other. An accurate measurement or calculation of MPC is pivotal for the correct description of the thermodynamical properties of magnetic materials [1,14,15]: The free energy will contain magnetic and vibrational contributions, often of the same magnitude. The MPC strength is maximal when spin waves (SWs) and elastic waves have the same frequency and wave number, i.e., when there is a crossing in the two dispersion curves [16]. At the intersection, the system shows neither a magnon nor a phonon, but rather a magnetoelastic excitation.

In the following, we present calculations of the combined effects of phononic (T_p) and magnonic (T_m) temperatures on the SW dispersion, stiffness, and Curie temperatures of Fe, Ni, and disordered $Ni_{81}Fe_{19}$ (permalloy or simply Py) by combining first-principles methods with model Hamiltonians. Inspired by Ref. [3], we present a theory that includes several effects on the magnetic exchange couplings. In addition to a first-principles description of MPC, we also take into account disorder within the virtual crystal approximation [17] (VCA)

*Present address: Toyota Motor Europe NV/SA, Advanced Technology Division, Zaventem 1930, Belgium; m.di.gennaro.bari@gmail.com

for the electronic ground state and vibrational properties calculation, and within the coherent potential approximation [18,19] (CPA) to calculate Heisenberg exchange integrals. This is nontrivial and adds chemical/structural disorder into the interplay between the magnetic and thermal excitations.

As a first step in our analysis, we consider the effect of T_p on the SW dispersion by means of linear spin-wave theory (LSWT). We then take into account the effects of thermal fluctuations in the magnetic system, within the quasiharmonic approximation and the atomistic spin dynamics (ASD) formalism [20,21], which allows for thermal noise and SW-SW interactions. In this way, we can consider separately the effects of the phonon and magnon temperatures, and study their influence on the SW energies, and implicitly gauge the MPC strength. We demonstrate the effect of the phonon temperature on the magnon dispersion, and show that, in Py, it competes with the spin fluctuations and renormalizes the acoustic mode. This introduces an unexpected nonmonotonic behavior of the magnetic response as a function of T, and defines an optimal temperature window for SW generation in spintronics applications.

Several previous works have taken a different approach by mixing spin and molecular dynamics potentials, combined with parametrized radially dependent magnetic exchange integrals, in particular by the Dudarev group [22]. This introduces an entropic effect on the magnetic exchange couplings, which then affects the total magnetic response in alloy systems. For Fe, they show very good agreement with experimental Curie temperatures. The exchange interactions are strongly simplified, assuming a $1/r^3$ functional dependence obtained from fitting two sets of calculated exchange integrals [3,23]. These exchange integrals are truncated to second-nearest neighbors, and do not take into account the detailed and oscillatory behavior of the exchange further out, which is relevant in many different magnetic materials. Here we consider the full range of exchange integrals, but consider the thermal vibrational effects in a more averaged way, as described below.

Our work goes in the same direction as two other first-principles approaches, namely, Refs. [4,24], trying to fill the gap between the fully ordered ferromagnetic and the disordered paramagnetic states. In this paper, we show explicitly how temperature reduces the magnetic exchange amongst the nearest neighbors and increases the coupling between remote ones. The effective MPC that we find in Permalloy is consistent with the "phonon drag" theory of the spin Seebeck effect (SSE) [25–27]. Very recently [28], the temperature dependence of the SW stiffness was determined experimentally for thin films using ferromagnetic resonance (FMR) measurements. We show below that the dependence at very low k (SW stiffness) only shows the magnon scattering, while the full dispersion should be sensitive to phonons as well. In general, thermal corrections improve the calculated Curie temperature with respect to experiment, but with very different magnitudes for different materials.

The paper is organized as follows: First, we present our formalism for the thermal dependence of the magnetic Heisenberg model, followed by the LSWT for disordered systems, and, finally, ASD and Curie Temperature calculations. The last sections report our numerical results, discussions, and conclusions.
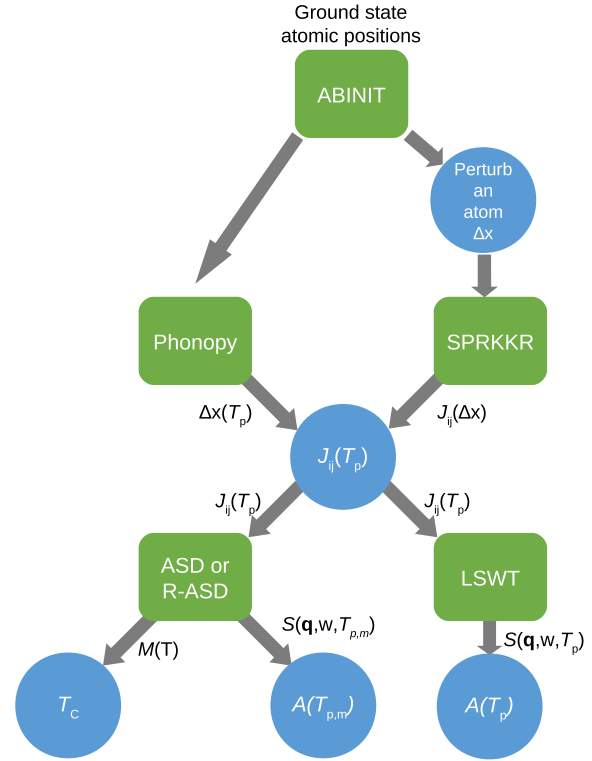

FIG. 1. A schematic showing the methodology used in this paper. The green squares represent the use of a code or method, the circles represent processing of data from a code/method, and the arrows show the transfer of data with the text next to the arrow representing what data is being transferred. All the symbols are explained in the Methods section.

II. METHODS

In this section, we detail how we calculate the phonons, magnons, and their effective coupling. The spin dynamics are treated with two formalisms, linear SW theory and ASD, which we have extended the former for disorder (Appendix) and both for finite lattice temperature.

Figure 1 shows the a schematic of the different approaches we have followed, which are explained in detail below. All structures are initially relaxed with ABINIT [29] to give the ground-state lattice parameters. This structure is fed into PHONOPY [30], whereby the average atomic displacements are calculated as a function of temperature. The same lattice parameters are also taken and an atom in the unit cell is perturbed by Δx to give a new structure which is subsequently used by SPRKKR [31]. The SPRKKR code then calculates the Heisenberg exchange parameters as a function of the perturbation. The size of the displacement as a function of temperature is combined with the displacement dependent J_{ij} are then combined to give $J_{ij}(T_p)$. These exchange constants are then used in both linear SW theory and atomistic spin dynamics (R-ASD for perturbed J_{ij} and ASD where the perturbation is zero). From (R)-ASD, the temperature-dependent magnetization and SWs are output and the Curie temperature and exchange stiffness calculated, respectively. The LSWT does not take into account changes in the length of the magnetization and therefore only looks at the effect of the phonon renormalization on the SWs (and then stiffness).

1. Thermal-dependent exchange integrals

We parametrize the magnetic Hamiltonian of the system, mapping electronic structure calculations on a Heisenberg Hamiltonian of the form

$$\mathcal{H} = - \sum_{\langle i\rho, j\eta \rangle} \mathcal{J}_{ij}^{\rho\eta} \mathbf{S}_i^{\rho} \cdot \mathbf{S}_j^{\eta}, \tag{1}$$

where i and j represent atomic sites and the ρ, η index refer to the atomic species. In the Hamiltonian Eq. (1), each species is treated with an explicit sublattice. In this framework, both CPA and VCA consider a disordered, single-atom species to deal with disorder. $\mathcal{J}_{ij}^{\rho\eta}$ is the exchange coupling between spins located at different sites and $\mathbf{S}^{\rho}$ are the spins associated with a given sublattice. The exchange-coupling constants are calculated as a function of the interatomic positions through the *ab initio* SPRKKR code [31].

The phonon bath temperature (T_p) is introduced by calculating, *ab initio*, the atomic mean-square thermal displacement $\sqrt{\langle u^2(T_p) \rangle}$ as implemented in PHONOPY [30] and obtained from the quasiharmonic approximation in the second quantization formalism. Chemical disorder is introduced for Py (1) in the $\mathcal{J}_{ij}^{\rho\eta}$ values using the CPA method, which returns all possible interactions among different sites and (2) in the phonons and thermal displacement using the VCA.

To calculate the effect of temperature on the exchange integrals, the Heisenberg exchange parameters, $\mathcal{J}_{ij}^{\rho\eta}$, are calculated for a set of distorted unit cells where the atom at the origin of the cell is displaced from its equilibrium position in steps from 1% to 5% of the cubic lattice constant, in the x direction. As the unit cells are all cubic, we only consider one displacement (along the x axis). Checks for forward and backward displacement, and with smaller steps (0.5%) were carried out to validate numerical aspects. For each displacement Δx, we calculate the exchange integrals $\mathcal{J}_{ij}^{\rho\eta}(\Delta x)$.

The results are then fit to a second-order polynomial with respect to the displacement:

$$\mathcal{J}_{ij}^{\rho\eta}(\Delta x) \simeq \mathcal{J}_{ij}^{\mathrm{F},\rho\eta}(0) + \frac{1}{2} \frac{\partial^2 \mathcal{J}_{ij}^{\mathrm{F},\rho\eta}}{\partial u^2} \Delta x^2. \tag{2}$$

By choosing $\Delta x = \sqrt{\langle u^2(T) \rangle}$, we obtain a temperature-dependent $\mathcal{J}_{ij}^{\rho\eta}(T_p) \equiv \mathcal{J}_{ij}^{\rho\eta}(\sqrt{\langle u^2(T_p) \rangle})$.

A different CPA formula incorporating thermal displacements and $\langle u^2(T) \rangle$ has recently been implemented in SPRKKR using a Debye approximation in Refs. [32,33] but does not yet allow for the calculation of the $\mathcal{J}_{ij}^{\rho\eta}$.

The cubic symmetry is broken by the finite displacement and subsequently restored on the exchange integrals by resymmetrizing the full $\mathcal{J}_{ij}$ matrix with the original cubic symmetry operations along x, y, and z (we assume uncorrelated thermal displacements). The renormalization is general, in that the $\mathcal{J}_{ij}$ variation propagates also to integrals relative to nondisplaced atoms—this is also a novelty compared to most previous calculations (except supercell approaches) which are two-body, and usually only vary $\mathcal{J}$ with the interatomic distance.

2. Linear spin-wave theory

We develop the theory of linear SWs for binary disordered systems into Appendix.

3. Atomistic spin dynamics

The dynamics of each spin is governed by the phenomenological Landau-Lifshitz-Gilbert equation (LLG) [34]:

$$\frac{d\mathbf{S}_i}{dt} = -\frac{\gamma_i}{(1+\lambda_i^2)\mu_i} \mathbf{S}_i \times [\mathbf{H}_i + \lambda_i \mathbf{S}_i \times \mathbf{H}_i], \tag{3}$$

where λ_i is the coupling to the *magnon* thermal bath which governs return to FM equilibrium. The amplitude of the magnetic moment is given by μ_i. The effective fields, $\mathbf{H}_i$, at the site i are determined using a Heisenberg Hamiltonian including exchange [as given in Eq. (1)] extended with anisotropy and Zeeman terms:

$$\mathcal{H}_{\mathrm{ASD}} = - \sum_{\langle i\rho, j\eta \rangle} \mathcal{J}_{ij}^{\rho\eta} \mathbf{S}_i^{\rho} \cdot \mathbf{S}_j^{\eta} - \sum_i K_i (\mathbf{S}_i^{\rho} \cdot \hat{\mathbf{n}})^2$$
$$- \sum_i \mu_i \mathbf{S}_i^{\rho} \cdot \mathbf{B}, \tag{4}$$

where K_i is the uniaxial anisotropy constant, assumed to be rather small in agreement with experimental and theoretical works [35]. $\hat{\mathbf{n}}$ is the direction of the easy axis taken here to be in the z direction. The final term in Eq. (4) is the Zeeman interaction with the applied magnetic field, $\mathbf{B}$. Based on a real space formalism, the magnetic moments, μ_i, are assumed to be localized on a given atomic site, i, with their time-dependence given by the phenomenological LLG Eq. (3). The effective field is given by the derivative of the Hamiltonian with respect to the spin,

$$\mathbf{H}_i = -\frac{\partial \mathcal{H}_{\mathrm{ASD}}}{\partial \mathbf{S}_i} + \boldsymbol{\zeta}_i, \tag{5}$$

and includes stochastic thermal fluctuations, $\boldsymbol{\zeta}_i$. These are included by incorporating a Langevin thermostat set to the desired magnonic temperature, T_m. In the present paper, the noise process is assumed to be white because of the timescale of equilibrium properties, where the heat bath (phonon or electron system) acts much faster than the spin system. The correlators of the process are defined through the fluctuation dissipation theorem as

$$\langle \zeta_i^{\alpha}(t) \rangle = 0,$$
$$\langle \zeta_i^{\alpha}(t) \zeta_j^{\beta}(t') \rangle = \frac{2\lambda_i k_{\mathrm{B}} T \mu_i}{\gamma_i} \delta_{ij} \delta_{\alpha\beta} \delta(t - t'). \tag{6}$$

The α, β represent cartesian (spin) components and i, j represent spin indices.

In ASD, unlike LSWT, disorder is taken into account by having a large supercell with 131, 072 single species atoms placed randomly on a lattice (fcc for Py), such that the desired composition is reached: Ni and Fe atoms do not occupy the same sites. For pure Fe and Ni, the values of the moments were $\mu_{\mathrm{Fe}} = 2.50\mu_{\mathrm{B}}$ and $\mu_{\mathrm{Ni}} = 0.655\mu_{\mathrm{B}}$, respectively. For Py, the magnetic moments were obtained from ground-state SPRKKR calculations and were $\mu_{\mathrm{Fe}} = 2.637\mu_{\mathrm{B}}$ and $\mu_{\mathrm{Ni}} = 0.628\mu_{\mathrm{B}}$. The phonon bath temperature is again included through the $\mathcal{J}_{ij}^{\rho\eta}(T_p)$ parameters. This gives a renormalized version of the ASD, to which we give the acronym R-ASD.

4. Curie temperature

To calculate the temperature-dependent magnetization (and subsequently the Curie temperature) the coupled LLG Eq. (3) is solved iteratively in the high damping limit and time averages of the components of the spin ensemble, $\mathbf{m}_\rho = \frac{1}{N_\rho} \sum_{i \in \rho}^{N_\rho} \mathbf{S}_i(t)$, are taken as in Ref. [36]. The system is initially equilibrated and a further period of time is then simulated to determine the average magnetization, which is monitored until convergence in both the mean and the variance is obtained.

5. Spin waves

The temperature-dependent magnon frequencies are determined by calculating the dynamic structure factor [37]:

$$S(\mathbf{k},\omega) = \frac{1}{N\sqrt{2\pi}} \sum_{\mathbf{r},\mathbf{r}'} e^{i\mathbf{k}\cdot(\mathbf{r}-\mathbf{r}')} \int_\infty^{+\infty} e^{-i\omega t} C(\mathbf{r}-\mathbf{r}',t) dt, \tag{7}$$

where $C(\mathbf{r}-\mathbf{r}',t) = \langle S^+(\mathbf{r},0)S^-(,\mathbf{r}',t)\rangle$ is the spin-spin correlation function of the transverse spin values (S_x and S_y). The stochastic thermal term allows the spin system to sample all modes and the resulting spectra are analyzed to determine the frequencies. The resulting magnon dispersion curves and magnetic response are shown in Figs. 5(b) and 5(d), and commented below.

6. Numerical details

Thermal displacements $\sqrt{\langle u^2(T)\rangle}$ as a function of T have been calculated from PHONOPY [30] in $2\times2\times2$ supercells. The electronic ground-state properties and forces have been calculated through density-functional theory using ABINIT [29]. The local density approximation and the generalized gradient approximation return very similar results for the electronic ground state as well as for phonon frequencies. The latter was employed with a set of FHI pseudopotentials [38], with a plane-wave energy cutoff set to 40 Ha, a gaussian electronic smearing of 1 meV, and a 12^3 Monkhorst-Pack grid to sample the Brillouin zone [39]. The ground-state energy was converged in all cases below 10^{-14} Ha. In the case of Py, the VCA was used to simulate disorder with the exact ratio (81% of nickel and 19% of iron) between species imposed. Harmonic phonon frequencies have also been calculated within density-functional perturbation theory as implemented in ABINIT [29] and agree well for these very simple one-atom unit cells. The phonon dispersion curve for VCA Py is shown in Fig. 2 in comparison with experimental results for disordered Ni$_3$Fe from Ref. [40].

The magnetic exchange integrals have been obtained using the spin-polarized relativistic Korringa-Kohn-Rostoker method as implemented in the Munich SPRKKR code [31,41], version 6.3. A generalized gradient approximation exchange-correlation functional is employed by Perdew-Burke-Ernzerhof [42]. A spin-polarized Scalar-Relativistic (SP-SREL) Hamiltonian was used with full potential on a Brillouin-zone grid of $22\times22\times22$ k-points, orbital momentum cutoff $l_{\max} = 3$, and 60 points on the complex energy path. All calculations were converged to 0.1 mRy of total energy. Temperature-dependent exchange integrals
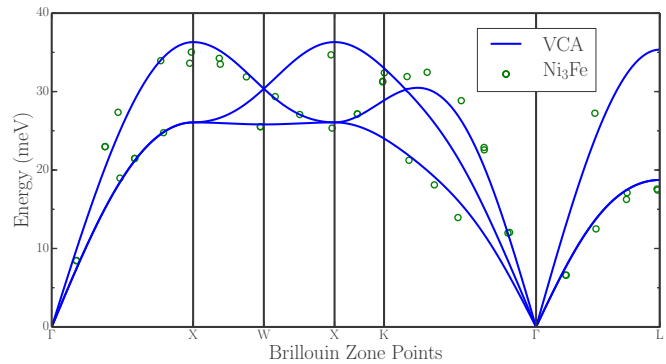

FIG. 2. Py phonons energies calculated within DFPT in the harmonic approximation from VCA compared to experimental results from Ref. [40].

$\mathcal{J}_{ij}^{\rho\eta}(T)$ are then obtained for each possible interaction of atoms in the central unit cell with all neighbors within a sphere of 3.5 times the lattice constant. Only one type of interaction is possible in pure Fe and Ni, whereas three different interactions are present in Py. Note that the chemical disorder in Py is described with a VCA approximation while the magnetic disorder comes from CPA. We used the conventional unit cells for the calculations: four-atom fcc for Ni and Py, and two-atom bcc for Fe.

Anharmonic effects are not considered in this paper, as a first step, justified as follows: (i) harmonic phonon frequencies agree with experimental results, (ii) the coefficient of thermal expansion for Py is modest at $12 \cdot 10^{-6}$ K^{-1} (Ref. [43] III/32A), and (iii) the fit of the $\mathcal{J}$ to a quadratic function of displacement has a residual error below 10^{-6} for all cases relative displacement of at most $\sim$5% at 1000 K. These effects could be included by (1) generalizing the renormalization of the magnetic coupling due to several atomic displacements and (2) by renormalizing the frequencies and mean-squared displacements; these avenues will be considered in the future, but given the final thermalization procedure, we expect the results would be qualitatively unchanged.

III. RESULTS

1. T-dependent Heisenberg exchange integrals

Temperature-dependent exchange interactions, as a function of the reduced distance between atoms and temperature, are displayed in Fig. 3 for Fe and Ni (three top and bottom) and for Py, Eq. (3). For Py, the variation of the magnetic exchange is shown in all three possible interactions in Py (Fe-Fe, Ni-Ni, and Fe-Ni). The amplitude of the ferromagnetic coupling can either increase or decrease with T_p and exchange integrals can even change sign. For Py, the amplitude of the exchange interaction between the first- and second-nearest neighbor interactions decreases with increasing T_p. Further out, the picture is more complex. The change in amplitude of $\mathcal{J}$ in Fe and Ni is much smaller than Py, in particular for the Fe–Fe and Fe–Ni intersublattice interactions. We postulate that within the CPA (with several species) the atomic displacement has a stronger effect on the charge transfers between Fe and Ni components, and thus on the local exchange integrals.
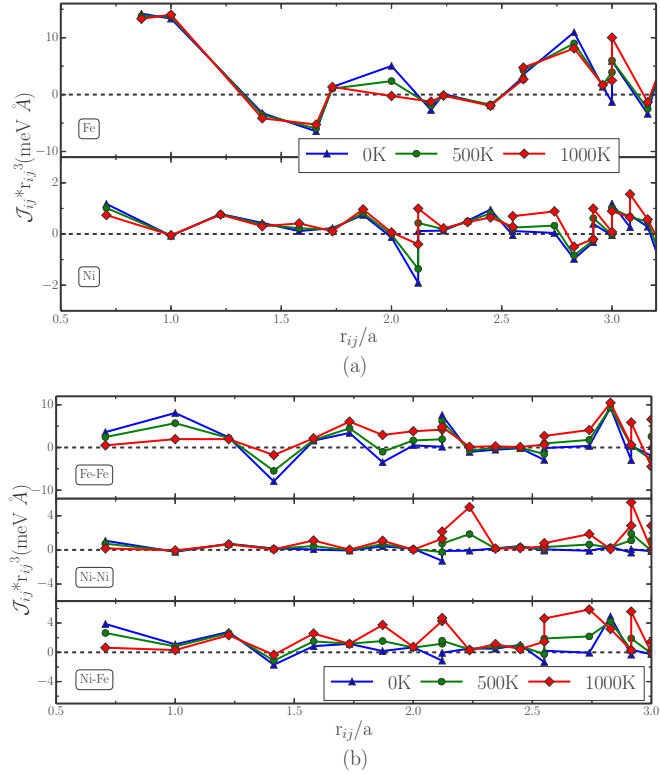
FIG. 3. Temperature-dependent Heisenberg exchange integrals (times reduced radius cubed) vs reduced radius and for different values of the phonon temperature. (a) Fe (top) and Ni (bottom) (b) Py. Three interactions are present: Fe-Fe (top), Ni-Ni (middle), and Ni-Fe (bottom).

The temperature dependence of the different neighbor interactions is also shown in Fig. 4 for the Fe-Fe, Ni-Ni, and Ni-Fe interactions in Py (N.B.: without the $1/r_{ij}^3$). It is important to notice that the first-neighbor interaction is generally the one most affected by the coupling with phonons (conforming with intuition), and that the $\mathcal{J}$ decrease in absolute value.
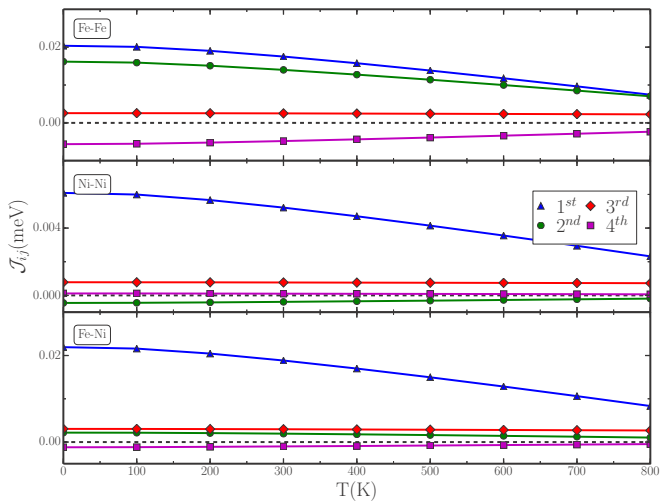

FIG. 4. Temperature dependence of the exchange interactions for the first-four neighbor shells shown explicitly for the Fe-Fe, Ni-Ni, and Ni-Fe interactions in Permalloy.

2. LSWT

To demonstrate the net effect of the phonon temperature on the SW frequencies in Py, we report the SW modes within LSWT (no thermal bath for the spins) in Fig. 5(a). In Py, there are two magnon modes [37], one optical and one acoustic, with a form determined by the mixture of the Ni-Ni, Fe-Fe, and Ni-Fe exchange [cf. Eqs. (A15) and (A14)]. We set $\langle S_0 \rangle = \langle S_1 \rangle = 1$ and $\nu_0 = 0.81$ and $\nu_1 = 0.19$ in the $\tilde{\mathcal{J}}_{ij}^{\rho\eta}$ definition. T_p produces an increase in magnon energies at small k, for both the acoustic and the optical branches, while there is almost no change at larger k.

3. Atomistic spin dynamics

The effect of the spin temperature on the SW spectrum is introduced with the ASD and R-ASD, and shown in Fig. 5(c). The resulting dispersion curve is quite different from that of the phonons in the LSWT case [Fig. 5(a)], showing the limits of the linear approximation, and in particular for higher temperatures. The inclusion of thermal spin fluctuations excites all eigenmodes of the system, and softens the magnons as the temperature of the thermostat increases. The acoustic branch is depressed at a frequency close to 200 meV [difference between 0 K and 600 K curves in Fig. 5(c)], near the Brillouin zone boundary, an effect which is much larger than the one found considering only phonon effects. The optical branch shows an opposite behavior in the whole Brillouin Zone ($\Gamma \rightarrow H$) compared to the LSWT, decreasing in frequency when $T = T_p = T_m$ increases. In Figs. 5(c) and 5(d), we present the easiest combination of temperatures of the different systems (phonon and magnon), setting $T_m = T_p$. This corresponds to the case where the phonons and magnons are completely equilibrated. Reference [25] shows that this is the case for the average global temperature in yttrium iron garnet upon pumping of heat into either bath. Other cases with $T_m \neq T_p$ are considered below (Fig. 7).

4. Spin-wave stiffness

To compare to experiments, we consider the SW stiffness D ($\omega_- \simeq Dk^2$ for small enough frequency), which is easier to access than the full dispersion. There are several ways to extract D: through $q \rightarrow 0$ fitting to the dispersion, through the temperature dependence of $M(T)$ presuming Bloch's law holds, or through the temperature dependence of FMR frequencies for standing waves in thin films, presuming the films have bulklike magnon dispersions. The latter two were used in Ref. [28] and yield very different values ($\sim$250 vs 450 meV Å^2) leading the authors to conclude (1) that Bloch's law does not hold and (2) that magnetism is probably itinerant. We agree with the former, but not the latter, as shown below. To determine D, we choose a fitting region up to $ka = 1.2$, as represented by the vertical dashed line in Figs. 5(a) and 5(c). The resulting $D(T)$ is shown in Fig. 5(b) for LSWT (phonon temperature only), and Fig. 5(d) for ASD (magnons only—blue triangles) and R-ASD (both magnons and phonons—green circles). As the real dispersion is never purely parabolic outside Γ, it is normal that different fits disagree.

We observe a monotonic increase of the stiffness with the temperature for LSWT. The near-neighbor exchange integrals soften in all three channels, whereas from the fifth neighbors out many harden (Fig. 4). We conclude that, as the temperature
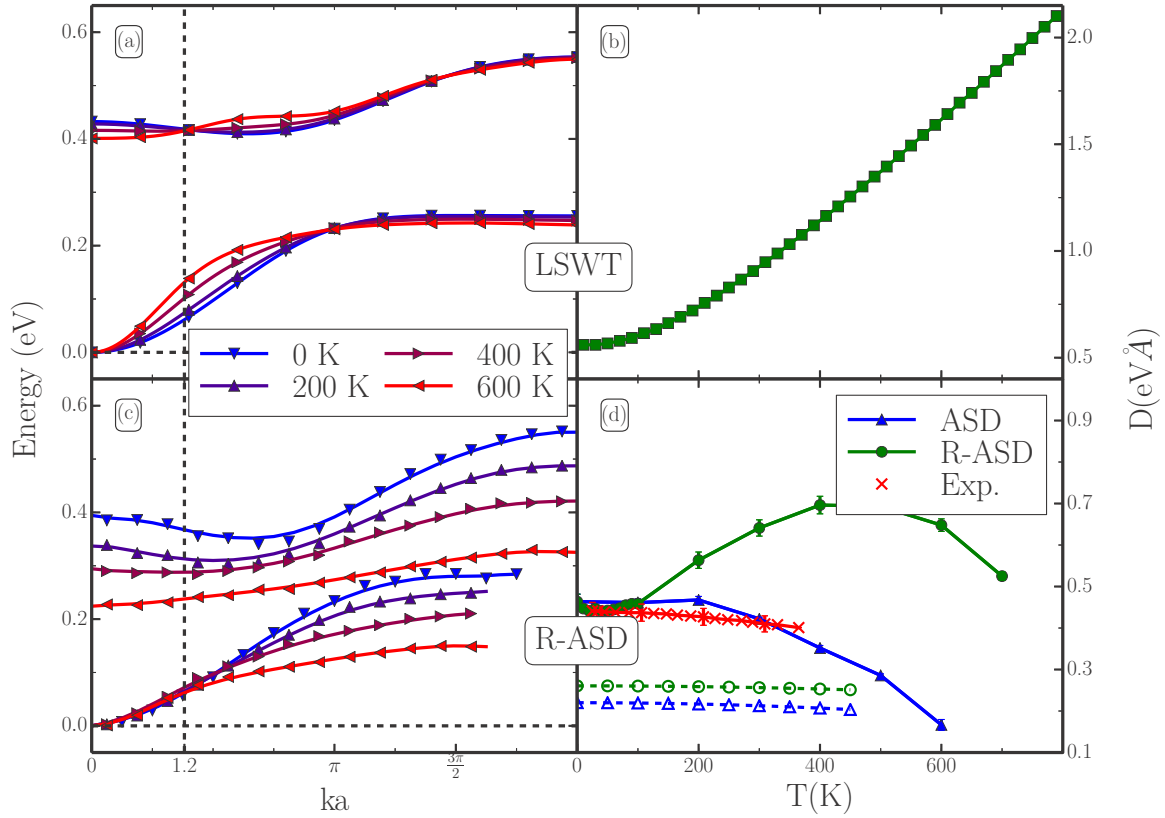
FIG. 5. Left: SW dispersion relation in Permalloy for a range of effective phonon temperatures calculated (a) within LSWT (no magnetic disorder) and (c) within R-ASD with both magnon and phonon contributions. Right: temperature dependence of the SW stiffness within LSWT (b) and using ASD (d) with renormalized exchange integrals (green circles) and with $\mathcal{J}_{ij}^{\rho\eta}$ values for $T_p = 0$ K (blue triangles). Dashed lines with open symbols in (d) are stiffness values extracted using a fit to Bloch's law (which underestimate, as found in Ref. [28]), the red crosses with error bars in (d) represent the fit of $D(T)$ in Ref. [28]. Phonon thermal effects are invisible in the experimental SW stiffness, which probes only the very long wavelength limit.

increases in LSWT, the weight of the first neighbors' $\mathcal{J}_{ij}$ becomes less important than at low temperature: the Phonons can have a strong effect on the long-range changes in $\mathcal{J}_{ij}$, which were not taken into account in previous work.

For ASD, when $T_p = 0$ [blue triangles in Fig. 5(d)] the stiffness monotonically decreases, while in the R-ASD, the introduction of finite T_p induces a nonmonotonic trend: for low T, the phonons increase D as for the LSWT, and at large enough T_m, the magnon dispersion must flatten, and D decreases. The agreement for the "straight" ASD with the experimental D (red crosses, panel d) is excellent, showing that purely magnon fluctuations reproduce the temperature dependence, and there is no need to invoke questions about itinerant magnetism in Py discussed in [28]. The stiffness, however, only contains very limited information in k: In the experimental setup, an FMR method uses a standing SW with a wavelength equal to the film thickness d (100 nm in Ref. [28]), and is therefore sensitive only to a single nonzero $k = 2\pi/d$, which is very close to Γ.

Our lattice thermal effect is strongest for the acoustic mode at the zone edge, and our k resolution at the zone center is limited by ASD supercell size and statistics. Due to (1) a limited phonon supercell and (2) single atom displacements plus resymmetrization, our calculations clearly overestimate the MPC at Γ (MPC should go to 0 at Γ due to phase space arguments for energy and momentum conservation). At larger k, the

SW dispersion becomes nonparabolic [as shown in Fig. 5(c)] and this is amplified by magnon and phonon perturbations. Both increase the higher order polynomial terms in k, but have opposite effects on the dispersion. The combination produces a nonmonotonic behavior in the magnon frequencies within the R-ASD. From this perspective, neutron scattering or a series of FMR measurements with smaller film thicknesses or higher harmonics of the standing waves would yield precious information on the SW dispersion, to test our proposal of a strong thermal effect on the SW dispersion far from the acoustic $k \sim \Gamma$. Figure 5(d) also shows fits of D from $M(T)$ as dashed lines. In this case, both ASD and R-ASD produce monotonically decreasing $D(T)$ and a strong underestimate as found experimentally in Ref. [28]. This difference reflects the limited validity of Bloch's law, both in theory and experiment: M is averaged over k and gives a less accurate value of D. Even at low T, fitting $M(T)$ is much less reliable than FMR, at least for Py. Compared to D, $M(T)$ always decreases with T, and M averages fluctuations over many length and timescales.

5. Magnetization and curie temperature

In this section, we discuss the effect of the temperature-dependent exchange interactions $\mathcal{J}_{ij}^{\rho\eta}(T_p)$ on the
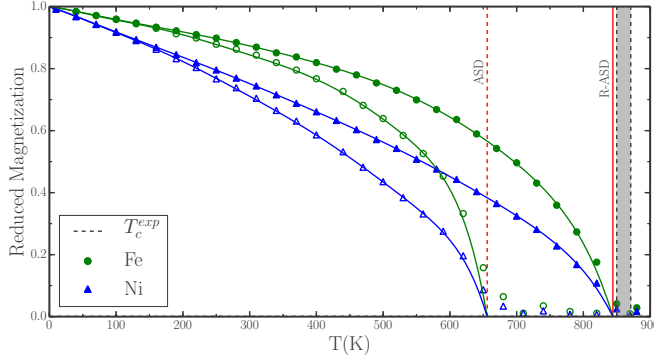
FIG. 6. Temperature-dependent magnetization curves of the two sublattices in Py: Fe (green circle) and Ni (blue triangles), calculated using ASD (open symbols) and temperature-dependent (closed symbols) exchange constants (R-ASD). Full lines are Taylor expansion fits [47] to extract the Curie temperatures (vertical lines). The grey area shows the range of Curie temperatures found experimentally [43,48], while the red vertical lines represent the Curie temperature from ASD (dashed) and R-ASD (full).

magnetization and Curie temperature, T_c. We have calculated the equilibrium magnetization $M(T)$ and show the results in Fig. 6. The ASD Curie temperature is derived as in Ref. [36]. We consider here the two cases: ASD [using $\mathcal{J}_{ij}^{\rho\eta}(0\,K)$ values—empty symbols in Fig. 6] and the R-ASD (using the temperature-dependent exchange constants, $\mathcal{J}_{ij}^{\rho\eta}(T_p)$, calculated previously with $T_m = T_p$). This magnetization contains the combined effect of the phononic and magnetic temperatures for the R-ASD case (closed symbols in Fig. 6).

The Curie temperatures from the different models used and from theoretical and experimental literature are given in Table I. We also report the result in the Mean Field Approximation (MFA) as in Ref. [44], considering both the unperturbed $\mathcal{J}_{ij}$ and the temperature-dependent $\mathcal{J}_{ij}(T_p)$. Phonon

TABLE I. Curie temperature (in K) calculated from MFA and ASD compared to previous results.

	Fe	Ni	Py
Other: MFA[b]	1414	397	
This: MFA	1725	455	796
This: MFA(T_p)	1662	452	867
Other: ASD[c]			650
This: ASD	1344	409	656
This: R-ASD	1333	415	844
Other: RPA[a]	950	350	
Other: R-RPA[g]	1057	634	
Monte Carlo[f]	1065	615	
Experiment	1043[d]	628.5[d]	850[e]
			871[d]

[a]Random phase approximation [49].
[b]MFA [49].
[c]ASD [45], Monte Carlo [50].
[d]Experimental data are from Ref. [43].
[e]Reference [48].
[f]Reference [50].
[g]Reference [51].

corrections lead to a slight decrease in the ASD calculated T_c for bcc Fe (from 1344 K to 1333 K), while it is increased for fcc Ni (from 409 K to 415 K). In both cases, introducing the phonon temperature induces an improvement, but only by a few percent or less.

In the case of disordered Py, our theoretical result outclasses previous methods: ASD returns $T_c = 656$ K using $\mathcal{J}_{ij}(0\,K)$, consistent with other works using CPA [45], while within R-ASD, T_c increases to 844 K, which considerably improves the agreement with experiments. This level of agreement may be fortuitous, but the amplitude of the correction shows that the renormalization of the exchange $\mathcal{J}_{ij}^{\rho\eta}$ with lattice temperature is crucial. A mean field calculation with $\mathcal{J}_{ij}^{\rho\eta}(0\,K)$ and $\mathcal{J}_{ij}^{\rho\eta}(T_p)$ also shows a strong variation of T_c, suggesting the details of the spin fluctuations are secondary.

We believe the difference in the order of magnitude of the phonon correction is due to two interrelated factors: (1) the presence of an optical magnon mode in Py enables more interactions with phonons and (2) our method is biased towards zone edge phonons, which seem to have a stronger coupling in Py, whereas in Fe and Ni the long wavelength phonons seem to be dominant. In the future, we will look at mode-resolved MPC and larger KKR unit cells, to verify these distinctions.

We note that the increase in the Curie temperature of Py due to the temperature-dependent exchange constants is already visible in their effect on the LSWT dispersion without magnetic disorder. In passing, Barker *et al.* [37] include the reduction of the magnetization directly in the LSWT, using a mean-field analysis, but their Curie temperature is strongly overestimated.

Finally, other corrections to the DFT/KKR+ASD framework are needed in general for a quantitative prediction of T_c, e.g., many-body effects in the $\mathcal{J}_{ij}^{\rho\eta}$ [46].

IV. DISCUSSION

In this section, we elaborate on the limitations of our method and directions for further study.

One important aspect of the MPC is adiabaticity: the (non)conservation of energy in the process of mutual scattering. A review of the problem of adiabaticity in itinerant ferromagnets can be found in Ref. [52]. We have assumed here that the fundamental postulate of their theory holds, i.e., a much faster timescale of the electronic degrees of freedom with respect to the slow magnetic system, and further postulate that correlations of the fast ionic motion are negligible. Both of these may be incorrect, and further work on the topic is very important for the fundamentals of MPC.

The Heisenberg model itself has limits, but should function for Fe and Py, which present localized magnetism. There is no good definition of localized moments in Ni, but empirically the Heisenberg model seems to work, and we include it for comparison: Our goal here is to investigate the interplay of vibrational and thermal effects, and they appear to work in similar ways in Ni.

A commonly proposed mechanism for the SSE is the propagation of out-of-equilibrium long-wavelength phonons in a crystalline substrate below the sample [27]. This enables a phonon-drag-like pumping of acoustic magnons in the magnetic material, and a resulting spin current which has a nonlocal origin. This is a difficult hypothesis to verify experimentally,
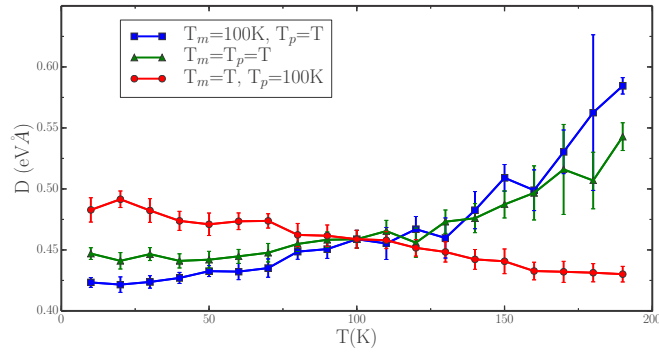
FIG. 7. Temperature-dependent exchange stiffness for three different nonequilibrium cases: (1) fixed magnetic (spin thermostat) temperature of $T_m = 100$ K and a varying phonon temperature, T_p (blue square points), (2) fixed phonon temperature $T_p = 100$ K and a varying magnetic (red diamond points), and (3) equal magnetic and phononic temperature (green circle points). The error bars are estimated from the error in the nonlinear least-squares fitting procedure.

and contributed to motivate the present study: Is the strength of the MPC sufficient to justify the observed spin current? In Ref. [26], a semiempirical model confirmed this hypothesis showing that at short wavelengths the magnetoelastic modes are mixed and scatter quickly, whereas at long wavelengths, scattering is weaker. We find in Py that spin fluctuations affect magnons of all wavelengths, whereas MPC is particularly strong for intermediate to short wavelengths ($k > 1.2/a$), which provides an important suggestion for future SSE models.

Our magnon dispersions implicitly contain the MPC in the temperature dependence of the magnons at different k, but also through the difference in temperature between the magnonic and phononic baths. For comparison, we have calculated of the stiffness, D, for three different cases, using the same low-k fitting of the SW spectrum as above. The first case is with a fixed magnetic temperature (the temperature of the spin thermostat) of $T_m = 100$ K and a varying phonon temperature, T_m (see blue squares in Fig. 7) given by the value on the x axis. The second case has a fixed phonon temperature, $T_p = 100$ K, and a varying temperature of the magnetic system, T_p (see red diamonds in Fig. 7). The third case corresponds to the case where the magnetic and phononic temperature are equal, $T_m = T_p$ [see green circles in Fig. 7, same in Fig. 5(d)]. The error bars are estimated from the error in the nonlinear least-squares fitting procedure. The trend of the three $D(T)$ curves is quite different, and offers, therefore, a way to distinguish between strong and weak MPC at low k by comparing to a "slow" adiabatic measurement. If D rises slowly or decreases with T_m, or if it increases strongly with T_p, then the coupling is weak and thermalization is difficult. We therefore strongly encourage a systematic experimental measurement of SW stiffnesses to verify the intrinsic MPC for other materials, and validate or expand the present explanation of the SSE.

V. CONCLUSION

A new method to calculate the thermal variation of magnetic exchange couplings is introduced, and the resulting change

in the SW frequencies is presented. The effects of both spin and lattice temperatures, T_m and T_p, are taken into account, using the ASD method and phonon-renormalized exchange interactions, respectively. We show that phonons weaken the exchange interaction at short distances and often harden for spins located further out, which has a nontrivial effect on the SW dispersion. T_p and T_m have competing effects on the magnon frequencies for Permalloy, which opens perspectives both for understanding and for tuning thermomagnetic behaviors. We compare the LSWT and mean-field approaches, which ignore SW-SW interactions, with the ASD which includes SW fluctuations. The temperature variation of the SW stiffness reflects exclusively the zone center dispersion, and is well described with spin fluctuations only. We find that the full dispersion relation changes due to both lattice and spin fluctuations, an effect which would require neutron scattering measurements of the dispersion to confirm. The agreement of our calculations with experimental T_c suggests that the recently measured simple variation of $D(T)$ belies the complex evolution of the full dispersion. SW stiffness values will depend strongly on the methods used to measure them, either relying on the dispersion, on Bloch's law, or using FMR measurements. We hope to stimulate further experimental investigation of the thermal evolution of SWs in Py and in other materials. This will provide a direct and simple quantification of the MPC, and is central to the understanding of spin-caloritronic effects.

Our theory is general and it can be applied to different crystal forms, magnetic cations, and variations of the components and alloy fractions. Beyond magnon spectrum changes with temperature, it also allows one to assess variations as a function of impurity concentration. These results open up important perspectives for tailoring alloys, without the need for costly nanostructuring, to obtain optimal spintronics and spin-caloritronic materials in a desired temperature window. Our results indicate that phonons can also lead to deviations from Bloch's law in measurements of the exchange stiffness [53]. Natural extensions include a fully phonon mode and wave-vector-dependent formalism to explore in more detail MPC from first principles.

APPENDIX: LINEAR SPIN-WAVE THEORY FOR DISORDERED MATERIALS

In this section, we derive explicitly the LSWT for an alloy, assuming a mixture of both Ni and Fe at each atomic site, i.e., the site and species exchange constants are weighted by the composition. We begin by linearizing the exchange part of the Hamiltonian Eq. (1) assuming that the x/y oscillations are small with respect to the spin moment in the quantization direction (taken to be the z axis). Writing the dot products in terms of the spin raising and lowering operators, $S^{\pm,\rho} = S_x^\rho \pm i S_y^\rho$, which are now species dependent:

$$\mathbf{S}_i^\rho \cdot \mathbf{S}_j^\eta = \tfrac{1}{2}\big[S_i^{+,\rho} S_j^{-,\eta} + S_i^{-,\rho} S_j^{+,\eta}\big] + S_i^{z,\rho} S_j^{z,\eta}, \quad \text{(A1)}$$

where ρ, η are the species. To describe the SW energies of a two-component disordered alloy system we first write the Hamiltonian explicitly for each set of interactions:

$$\mathcal{H} = \sum_i \sum_j \tilde{\mathcal{J}}_{ij}^{00} \mathbf{S}_i^0 \cdot \mathbf{S}_j^0 + \sum_i \sum_j \tilde{\mathcal{J}}_{ij}^{01} \mathbf{S}_i^0 \cdot \mathbf{S}_j^1$$
$$+ \sum_i \sum_j \tilde{\mathcal{J}}_{ij}^{10} \mathbf{S}_i^1 \cdot \mathbf{S}_j^0 + \sum_i \sum_j \tilde{\mathcal{J}}_{ij}^{11} \mathbf{S}_i^1 \cdot \mathbf{S}_j^1, \quad \text{(A2)}$$

where the superscripts (0,1) correspond to each species pair (ρ, η). We assume that the magnetic moments of each species occupy the same sites (see below) and the $\mathcal{J}_{ij}^{\rho\eta}$ are corrected in the spirit of a VCA to account for composition, $\tilde{\mathcal{J}}_{ij}^{\rho\eta} = \mathcal{J}_{ij}^{\rho\eta} \nu_\rho$, where ν_ρ is the percentage of the species, ρ. Writing the $\mathbf{S}_i^\rho \cdot \mathbf{S}_j^\eta$ products in terms of the species dependent spin raising and lowering operators, the Hamiltonian becomes

$$\mathcal{H} = \sum_i \sum_j \tilde{\mathcal{J}}_{ij}^{00} \left\{ \frac{1}{2}\big[S_i^{+,0} S_j^{-,0} + S_i^{-,0} S_j^{+,0}\big] + S_i^{z,0} S_j^{z,0} \right\}$$
$$+ \sum_i \sum_j \tilde{\mathcal{J}}_{ij}^{01} \left\{ \frac{1}{2}\big[S_i^{+,0} S_j^{-,1} + S_i^{-,0} S_j^{+,1}\big] + S_i^{z,0} S_j^{z,1} \right\}$$
$$+ \sum_i \sum_j \tilde{\mathcal{J}}_{ij}^{10} \left\{ \frac{1}{2}\big[S_i^{+,1} S_j^{-,0} + S_i^{-,1} S_j^{+,0}\big] + S_i^{z,1} S_j^{z,0} \right\}$$
$$+ \sum_i \sum_j \tilde{\mathcal{J}}_{ij}^{11} \left\{ \frac{1}{2}\big[S_i^{+,1} S_j^{-,1} + S_i^{-,1} S_j^{+,1}\big] + S_i^{z,1} S_j^{z,1} \right\}. \quad \text{(A3)}$$

As we are neglecting the thermal effects arising from fluctuations of the magnetic moments, we take the low temperature approximation for the Holstein-Primakoff transformations [54]:

$$S_i^{+,0} \approx \hbar\sqrt{2S}\, a_i^{+,0}, \quad S_i^{-,0} \approx \hbar\sqrt{2S}\, a_i^{-,0}. \quad \text{(A4)}$$

For ease of notation, we take $\hbar = 1$ and absorb the spin value, S, in the exchange constant (i.e., setting $S = 1$). The transverse components in Eq. (A3) are then replaced by the low temperature Holstein-Primakoff transformation and we

use the relation $S_i^{z,\rho} = S - \hat{n}_i^\rho$, where $\hat{n}_i^\rho = a_i^{+,\rho} a_i^{-,\rho}$ is the number operator. Then, $S_i^z S_j^z = (S - \hat{n}_i^\rho)(S - \hat{n}_j^\eta)$. We neglect terms beyond first order, and note that the pure powers of S only add an arbitrary constant to the Hamiltonian. Furthermore, we can relabel the sum over j by introducing the $\boldsymbol{\delta}$ vector, which is the translation between i and a neighbor, j, $\sum_i \sum_j \rightarrow \sum_{ij} \rightarrow \sum_{i\delta}$. For a disordered alloy with only one type of site, we have $\mathcal{J}_{i,j} = \mathcal{J}_{i,i+\delta} = \mathcal{J}_\delta$ depending on the relative displacement *only*. Thus we can write the Hamiltonian:

$$\mathcal{H} = \sum_{i,\delta} \tilde{\mathcal{J}}_\delta^{00} \big\{ a_i^{-,0} a_{i+\delta}^{+,0} + a_i^{+,0} a_{i+\delta}^{-,0} - a_i^{+,0} a_i^{-,0} - a_{i+\delta}^{+,0} a_{i+\delta}^{-,0} \big\}$$
$$+ \sum_{i,\delta} \tilde{\mathcal{J}}_\delta^{01} \big\{ a_i^{-,0} a_{i+\delta}^{+,1} + a_i^{+,0} a_{i+\delta}^{-,1} - a_i^{+,0} a_i^{-,0} - a_{i+\delta}^{+,1} a_{i+\delta}^{-,1} \big\}$$
$$+ \sum_{i,\delta} \tilde{\mathcal{J}}_\delta^{10} \big\{ a_i^{-,1} a_{i+\delta}^{+,0} + a_i^{+,1} a_{i+\delta}^{-,0} - a_i^{+,1} a_i^{-,1} - a_{i+\delta}^{+,0} a_{i+\delta}^{-,0} \big\}$$
$$+ \sum_{i,\delta} \tilde{\mathcal{J}}_\delta^{11} \big\{ a_i^{-,1} a_{i+\delta}^{+,1} + a_i^{+,1} a_{i+\delta}^{-,1} - a_i^{+,1} a_i^{-,1} - a_{i+\delta}^{+,1} a_{i+\delta}^{-,1} \big\}. \quad \text{(A5)}$$

We can then transform to Fourier space through $a_i^{\pm,\rho} = \sum_{\mathbf{k}} e^{\mp i\mathbf{k}\cdot\mathbf{r}} a_{\mathbf{k}}^{\pm,\rho}$. Substituting these into Eq. (A5) gives (for readability we write just the first term, $\rho = \eta = 0$)

$$\mathcal{H}^{00} = \sum_{i\delta\mathbf{k}\mathbf{k}'} \tilde{\mathcal{J}}_\delta^{00} \big[e^{-i(\mathbf{k}-\mathbf{k}')\cdot\mathbf{r}_i} e^{+i\mathbf{k}'\cdot\boldsymbol{\delta}} a_{\mathbf{k}}^{+,0} a_{\mathbf{k}'}^{-,0}$$
$$+ e^{+i(\mathbf{k}-\mathbf{k}')\cdot\mathbf{r}_i} e^{-i\mathbf{k}'\cdot\boldsymbol{\delta}} a_{\mathbf{k}}^{-,0} a_{\mathbf{k}'}^{+,0}$$
$$+ e^{-i(\mathbf{k}-\mathbf{k}')\cdot\mathbf{r}_i} a_{\mathbf{k}}^{+,0} a_{\mathbf{k}'}^{-,0}$$
$$+ e^{-i(\mathbf{k}-\mathbf{k}')\cdot(\mathbf{r}_i+\boldsymbol{\delta})} a_{\mathbf{k}}^{+,0} a_{\mathbf{k}'}^{-,0} \big]. \quad \text{(A6)}$$

Sums over i cause all terms to vanish unless $\mathbf{k} = \mathbf{k}'$ [54] and thus the sum becomes

$$\mathcal{H}^{00} = \sum_{\mathbf{k}\delta} \tilde{\mathcal{J}}_\delta^{00} \big[e^{-i\mathbf{k}\cdot\boldsymbol{\delta}} a_{\mathbf{k}}^{+,0} a_{\mathbf{k}}^{-,0} + e^{+i\mathbf{k}\cdot\boldsymbol{\delta}} a_{\mathbf{k}}^{-,0} a_{\mathbf{k}}^{+,0} - 2 a_{\mathbf{k}}^{+,0} a_{\mathbf{k}}^{-,0} \big]. \quad \text{(A7)}$$

We use the identity $[a^+, a^-] = 1$ and define $\gamma_{\mathbf{k}} = \sum_\delta e^{-i\mathbf{k}\cdot\boldsymbol{\delta}}$ and $\tilde{\mathcal{J}}_{\mathbf{k}} = \sum_\delta \tilde{\mathcal{J}}_\delta e^{-\mathbf{k}\cdot\boldsymbol{\delta}}$. For crystals with a center of inversion symmetry (fcc, bcc), $\gamma_{\mathbf{k}} = \gamma_{-\mathbf{k}}$, simplifying Eq. (A7) to

$$\mathcal{H}^{00} = \sum_{\mathbf{k}\delta} \tilde{\mathcal{J}}_\delta^{00} \big[\gamma_{\mathbf{k}} a_{\mathbf{k}}^{+,0} a_{\mathbf{k}}^{-,0} + \gamma_{\mathbf{k}} a_{\mathbf{k}}^{-,0} a_{\mathbf{k}}^{+,0} - 2 a_{\mathbf{k}}^{+,0} a_{\mathbf{k}}^{-,0} \big]$$
$$= \sum_{\mathbf{k}\delta} \tilde{\mathcal{J}}_\delta^{00} \big[2\gamma_{\mathbf{k}} a_{\mathbf{k}}^{+,0} a_{\mathbf{k}}^{-,0} + \gamma_{\mathbf{k}} - 2 a_{\mathbf{k}}^{+,0} a_{\mathbf{k}}^{-,0} \big]. \quad \text{(A8)}$$

Again, we ignore the arbitrary constant $\sum_{\mathbf{k}} \gamma_{\mathbf{k}}$, and take the sum over $\boldsymbol{\delta}$ inside. The Hamiltonian given by Eq. (A8) becomes

$$\mathcal{H}^{00} = 2 \sum_{\mathbf{k}} \big(\tilde{\mathcal{J}}_{\mathbf{k}}^{00} - \tilde{\mathcal{J}}_0^{00} \big) a_{\mathbf{k}}^{+,0} a_{\mathbf{k}}^{-,0}. \quad \text{(A9)}$$

Terms for $\mathcal{H}^{01}$, $\mathcal{H}^{10}$, and $\mathcal{H}^{11}$ can be derived in a similar way. For brevity, they have not been shown explicitly here but we note that we can write the Hamiltonian as a matrix product:

$$\mathcal{H} = \sum_{\mathbf{k}} a_{\mathbf{k}}^{+,T} M a_{\mathbf{k}}^-, \quad \text{(A10)}$$

where M is a 2×2 matrix containing the appropriate exchange constants and

$$a^{\pm}_{\mathbf{k}} = \begin{bmatrix} a^{\pm,0}_{\mathbf{k}} \\ a^{\pm,1}_{\mathbf{k}} \end{bmatrix}. \quad (A11)$$

The Hamiltonian matrix is rewritten using a Bogoliubov transformation [55], which now *mixes* the excitations associated with Ni-Ni, Fe-Fe, and Ni-Fe exchange interactions:

$$a^{\pm,0}_{\mathbf{k}} = u_{\mathbf{k}} \alpha^{\pm}_{\mathbf{k}} + v_{\mathbf{k}} \beta^{\mp}_{\mathbf{k}},$$
$$a^{\pm,1}_{\mathbf{k}} = u_{\mathbf{k}} \beta^{\pm}_{\mathbf{k}} + v_{\mathbf{k}} \alpha^{\mp}_{\mathbf{k}}. \quad (A12)$$

With this transform the Hamiltonian can then be written as

$$\mathcal{H} = \sum_{\mathbf{k}} [\alpha^{+}_{\mathbf{k}} \beta^{+}_{\mathbf{k}}] \mathcal{M}_{\mathbf{k}} \begin{bmatrix} \alpha^{-}_{\mathbf{k}} \\ \beta^{-}_{\mathbf{k}} \end{bmatrix}. \quad (A13)$$

The elements of the matrix $\mathcal{M}_{\mathbf{k}}$ can be found by comparing coefficients of the $a^{\pm,\rho}_{\mathbf{k}}$:

$$\mathcal{M}_{\mathbf{k}} = \begin{bmatrix} \Omega_{\mathbf{k},0}\langle S_0 \rangle + \Xi_{\mathbf{k},00} & \Xi_{\mathbf{k},01} \\ \Xi_{\mathbf{k},10} & \Omega_{\mathbf{k},1}\langle S_1 \rangle + \Xi_{\mathbf{k},01} \end{bmatrix}, \quad (A14)$$

where $\Omega_{\mathbf{k}\rho} = \frac{\gamma}{\mu_{\rho}} \sum_{\mathbf{R}} \tilde{\mathcal{J}}^{\rho\rho}_{ij}(\mathbf{R})[1 - \exp(i\mathbf{k} \cdot \mathbf{R})]$ is the SW frequency of the individual species (the two possible sublattices). γ is the gyromagnetic ratio, μ_{ρ} are the spin moment amplitudes, and $\Xi_{\mathbf{k},\rho\eta} = \frac{\gamma}{\mu_{\rho}} \sum_{\mathbf{R}} \tilde{\mathcal{J}}^{\rho\eta}_{ij}(\mathbf{R})\langle S_{\eta} \rangle$. $\langle \cdot \rangle$ represents the equilibrium value of reduced magnetisations for each species (normalised to 1 at $T = 0$ K). Here we ignore spin fluctuations and these values are fixed to 1. We could artificially introduce a temperature dependence of the magnetization in the LSWT but we choose not to as the ASD gives a better account of spin fluctuations as it allows for SW interactions.

Upon diagonalization, the solutions to the eigenvalue equation are given by

$$\omega_{\pm}(\mathbf{k}) = \frac{1}{2}[\text{Tr}\,\mathcal{M}_{\mathbf{k}} \pm \sqrt{(\text{Tr}\,\mathcal{M}_{\mathbf{k}})^2 - 4\det[\mathcal{M}_{\mathbf{k}}]}], \quad (A15)$$

where $\pm$ corresponds to the upper $(+)$ and lower $(-)$ magnon branches, det is the determinant. The resulting magnon dispersion curves and magnetic response are shown in Figs. 5(a) and 5(c) and commented in the main text.

[1] D. J. Sanders and D. Walton, Phys. Rev. B **15**, 1489 (1977).

[2] E. Abrahams and C. Kittel, Phys. Rev. **88**, 1200 (1952).

[3] R. F. Sabiryanov and S. S. Jaswal, Phys. Rev. Lett. **83**, 2062 (1999).

[4] F. Körmann, B. Grabowski, B. Dutta, T. Hickel, L. Mauger, B. Fultz, and J. Neugebauer, Phys. Rev. Lett. **113**, 165503 (2014).

[5] J. Fransson, D. Thonig, P. F. Bessarab, S. Bhattacharjee, J. Hellsvik, and L. Nordström, Phys. Rev. Mater. **1**, 074404 (2017).

[6] K. Uchida, H. Adachi, T. Ota, H. Nakayama, S. Maekawa, and E. Saitoh, Appl. Phys. Lett. **97**, 172505 (2010).

[7] K. Uchida, S. Takahashi, K. Harii, J. Ieda, W. Koshibae, K. Ando, S. Maekawa, and E. Saitoh, Nature **455**, 778 (2008).

[8] K. Uchida, T. Ota, H. Adachi, J. Xiao, T. Nonaka, Y. Kajiwara, G. E. W. Bauer, S. Maekawa, and E. Saitoh, J. Appl. Phys. **111**, 103903 (2012).

[9] H. Adachi, K. Uchida, E. Saitoh, and S. Maekawa, Rep. Prog. Phys. **76**, 036501 (2013).

[10] J. Flipse, F. K. Dejene, D. Wagenaar, G. E. W. Bauer, J. Ben Youssef, and B. J. van Wees, Phys. Rev. Lett. **113**, 027601 (2014).

[11] G. E. W. Bauer, E. Saitoh, and B. J. van Wees, Nat. Mater. **11**, 391 (2012).

[12] S. R. Boona, R. C. Myers, and J. P. Heremans, Energy Environ. Sci. **7**, 885 (2014).

[13] J. de la Venta, S. Wang, T. Saerbeck, J. Ramírez, I. Valmianski, and I. K. Schuller, Appl. Phys. Lett. **104**, 062410 (2014).

[14] J. Van Kranendonk and J. H. Van Vleck, Rev. Mod. Phys. **30**, 1 (1958).

[15] H. Sato, Prog. Theor. Phys. **13**, 119 (1955).

[16] C. Kittel, Phys. Rev. **110**, 836 (1958).

[17] L. Bellaiche and D. Vanderbilt, Phys. Rev. B **61**, 7877 (2000).

[18] P. Soven, Phys. Rev. **156**, 809 (1967).

[19] H. Ebert, B. Drittler, and H. Akai, J. Magn. Magn. Mater. **104–107**, Part 1, 733 (1992).

[20] B. Skubic, J. Hellsvik, L. Nordström, and O. Eriksson, J. Phys.: Condens. Matter **20**, 315203 (2008).

[21] D. Berkov, in *The Handbook of Magnetism and Advanced Magnetic Materials*, edited by H. Kronmüller and S. Parkin (Wiley, Sussex, 2006).

[22] P.-W. Ma, C. H. Woo, and S. L. Dudarev, Phys. Rev. B **78**, 024434 (2008).

[23] S. Morán, C. Ederer, and M. Fähnle, Phys. Rev. B **67**, 012407 (2003).

[24] Y. Liu, Z. Yuan, R. J. H. Wesselink, A. A. Starikov, M. van Schilfgaarde, and P. J. Kelly, Phys. Rev. B **91**, 220405 (2015).

[25] M. Agrawal, V. I. Vasyuchka, A. A. Serga, A. D. Karenowska, G. A. Melkov, and B. Hillebrands, Phys. Rev. Lett. **111**, 107204 (2013).

[26] A. Rückriegel, P. Kopietz, D. A. Bozhko, A. A. Serga, and B. Hillebrands, Phys. Rev. B **89**, 184413 (2014).

[27] H. Adachi, K. Uchida, E. Saitoh, J.-i. Ohe, S. Takahashi, and S. Maekawa, Appl. Phys. Lett. **97**, 252506 (2010).

[28] Y. Yin, M. Ahlberg, P. Dürrenfeld, Y. Zhai, R. K. Dumas, and J. Åkerman, IEEE Magn. Lett. **8**, 1 (2017).

[29] X. Gonze, F. Jollet, F. Abreu Araujo, D. Adams, B. Amadon, T. Applencourt, C. Audouze, J.-M. Beuken, J. Bieder, A. Bokhanchuk, E. Bousquet, F. Bruneval, D. Caliste, M. Côté, F. Dahm, F. Da Pieve, M. Delaveau, M. Di Gennaro, B. Dorado, C. Espejo, G. Geneste, L. Genovese, A. Gerossier, M. Giantomassi, Y. Gillet, D. Hamann, L. He, G. Jomard, J. Laflamme Janssen, S. Le Roux, A. Levitt, A. Lherbier, F. Liu, I. Lukačević, A. Martin, C. Martins, M. Oliveira, S. Poncé, Y. Pouillon, T. Rangel, G.-M. Rignanese, A. Romero, B. Rousseau, O. Rubel, A. Shukri, M. Stankovski, M. Torrent, M. Van Setten, B. Van Troeye, M. Verstraete, D. Waroquiers, J. Wiktor, B. Xu, A. Zhou, and J. Zwanziger, Comput. Phys. Commun. **205**, 106 (2016).

[30] A. Togo, F. Oba, and I. Tanaka, Phys. Rev. B **78**, 134106 (2008).

[31] H. Ebert, D. Ködderitzsch, and J. Minár, Rep. Prog. Phys. **74**, 096501 (2011).

[32] H. Ebert, S. Mankovsky, D. Ködderitzsch, and P. J. Kelly, Phys. Rev. Lett. **107**, 066603 (2011).

[33] D. Ködderitzsch, K. Chadova, J. Minár, and H. Ebert, New J. Phys. **15**, 053009 (2013).

[34] T. Gilbert, IEEE Trans. Magn. **40**, 3443 (2004).

[35] L. F. Yin, D. H. Wei, N. Lei, L. H. Zhou, C. S. Tian, G. S. Dong, X. F. Jin, L. P. Guo, Q. J. Jia, and R. Q. Wu, Phys. Rev. Lett. **97**, 067203 (2006).

[36] T. A. Ostler, R. F. L. Evans, R. W. Chantrell, U. Atxitia, O. Chubykalo-Fesenko, I. Radu, R. Abrudan, F. Radu, A. Tsukamoto, A. Itoh, A. Kirilyuk, T. Rasing, and A. V. Kimel, Phys. Rev. B **84**, 024407 (2011).

[37] J. Barker, U. Atxitia, T. A. Ostler, O. Hovorka, R. W. Chantrell, O. Chubykalo-Fesenko, and R. W. Chantrell, Sci. Rep. **3**, 3262 (2013).

[38] X. Gonze, R. Stumpf, and M. Scheffler, Phys. Rev. B **44**, 8503 (1991).

[39] H. J. Monkhorst and J. D. Pack, Phys. Rev. B **13**, 5188 (1976).

[40] E. Hallaman and B. Brockhouse, Can. J. Phys. **47**, 1117 (1969).

[41] H. Ebert, M. Battocletti, D. Benea, S. Bornemann, J. Braun, S. Chadov, M. Deng, H. Freyer, T. Huhne, D. Koöderitzsch *et al.*, The Munich SPR-KKR package, version 6.3, http://ebert.cup.uni-muenchen.de/SPRKKR.

[42] J. P. Perdew, K. Burke, and M. Ernzerhof, Phys. Rev. Lett. **77**, 3865 (1996).

[43] J. Bass, J. S. Dugdale, C. L. Foiles, and A. Myers, in *Electrical Resistivity, Thermoelectrical Power and Optical Properties*, edited by K.-H. Hellwege and J. L. Olsen (Springer, Berlin, Heidelberg, 1985), Vol. 15b.

[44] E. Şaşıoğlu, L. M. Sandratskii, and P. Bruno, Phys. Rev. B **70**, 024427 (2004).

[45] D. Hinzke, U. Atxitia, K. Carva, P. Nieves, O. Chubykalo-Fesenko, P. M. Oppeneer, and U. Nowak, Phys. Rev. B **92**, 054412 (2015).

[46] E. Şaşıoğlu, A. Schindlmayr, C. Friedrich, F. Freimuth, and S. Blügel, Phys. Rev. B **81**, 054434 (2010).

[47] N. Kazantseva, D. Hinzke, U. Nowak, R. W. Chantrell, U. Atxitia, and O. Chubykalo-Fesenko, Phys. Rev. B **77**, 184428 (2008).

[48] S. Mathias, C. La-O-Vorakiat, P. Grychtol, P. Granitzka, E. Turgut, J. M. Shaw, R. Adam, H. T. Nembach, M. E. Siemens, S. Eich, C. M. Schneider, T. J. Silva, M. Aeschlimann, M. M. Murnane, and H. C. Kapteyn, Proc. Natl. Acad. Sci. USA **109**, 4792 (2012).

[49] M. Pajda, J. Kudrnovský, I. Turek, V. Drchal, and P. Bruno, Phys. Rev. B **64**, 174402 (2001).

[50] A. V. Ruban, S. Khmelevskyi, P. Mohn, and B. Johansson, Phys. Rev. B **75**, 054402 (2007).

[51] P. Bruno, Phys. Rev. Lett. **90**, 087205 (2003).

[52] S. V. Halilov, H. Eschrig, A. Y. Perlov, and P. M. Oppeneer, Phys. Rev. B **58**, 293 (1998).

[53] M. Mulazzi, A. Chainani, Y. Takata, Y. Tanaka, Y. Nishino, K. Tamasaku, T. Ishikawa, T. Takeuchi, Y. Ishida, Y. Senba, H. Ohashi, and S. Shin, Phys. Rev. B **77**, 224425 (2008).

[54] D. D. Stancil and A. Prabhakar, *Spin Waves Theory and Applications* (Springer, New York, 2009).

[55] N. N. Bogoliubov, J. Phys. (USSR) **11**, 23 (1947).